Dynamic features of viscoelastic fluid counter flows

Igor Mackarov

Bogdanovich st. 55/232, Minsk, 220123, Belarus
Mackarov@gmx.net

ABSTRACT

The paper presents the results of numerical study of the acceleration/stabilization phase of counter flows of Oldroyd-B and De Witt viscoelastic fluids. It is shown that the flow patterns at this stage often involve oscillatory phenomena, in particular, periodic changes of the flow speed in value and direction.

Comparison of the flows considered with the initial acceleration phases of simpler viscoelastic fluid flows has made it possible to come to the conclusion that on the non-stationary stabilization phase a viscoelastic fluid flow has a wave nature which is underlain by the role of the fluid elasticity involving propagation of the disturbances, cursed by the walls and the pressure gradient, across the flow with some speed depending on both the Weissenberg and the Reynolds numbers.

INTRODUCTION

One of the characteristic features of counter flows of viscoelastic fluids within cross-channels is the fluid high stretches in the vicinity of the stagnation central point. Admittedly, such stretches are a reason of the specific dynamic features such as patterns of secondary vortex-like flows, and loss of the flow symmetry[1,2,3]. At the same time, it should be mentioned that in some investigations of the viscoelastic fluid flows within similar regions absence of such phenomena was also reported[4]. Evidently, such a variety takes place because the characteristics of this kind of flows are very sensitive to an experiment conditions, or to the details of the problem statement in the case of the numerical simulation.

In the present research we focus on the *acceleration/stabilization* phase of the viscoelastic fluid flow within cross-channels applying physically realistic boundary conditions (for inlet and outlet pressures). This is the continuation of the research reported earlier[5].

PROBLEM STATEMENT

To wider describe a fluid rheological behavior, in addition to the widely used *UCM* (Upper Convective Maxwell) model and its generalization, the *Oldroyd-B* model, another representative of the generalized Maxwell models family, the *De Witt* model (with the Jauman derivative), was considered.

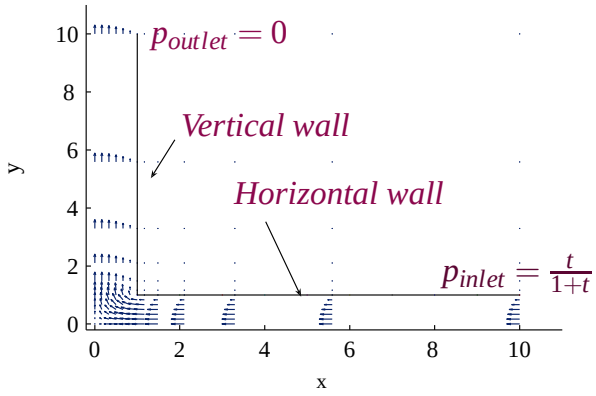

Figure 1. General layout of the counter flows (a quarter domain).

Due to the domain symmetry, the problem was solved in the quarter domain shown in Fig. 1 (previously[5], for the sake of analysis of the solution stability, a similar problem was also solved in the whole domain, the solution ob-

tained turned out quite symmetric and close to the one in a quarter domain).

The momentum and continuity equations

$$\frac{\partial v_i}{\partial t} + v_j \frac{\partial v_i}{\partial x_j} = -\frac{\partial p}{\partial x_i} + \frac{\partial \sigma_{ij}}{\partial x_j} \tag{1}$$

$$\frac{\partial v_i}{\partial x_i} = 0 \tag{2}$$

(here and later we mean summation on the repeated indexes $i, j = 1,2$) were solved together with each of the two rheological models using the dimensionless variables normalized on the problem natural scales:

Oldroyd-B model:

$$\sigma = \sigma^s + \sigma^p \tag{3}$$

$$\sigma^s_{ij} = \frac{1}{Re_s}\left(\frac{\partial v_i}{\partial x_j} + \frac{\partial v_j}{\partial x_i}\right) \tag{4}$$

$$\frac{D\sigma^p_{ij}}{Dt} + \frac{1}{Wi}\sigma^p_{ij} = \frac{1}{Wi\,Re_p}\left(\frac{\partial v_i}{\partial x_j} + \frac{\partial v_j}{\partial x_i}\right) \tag{5}$$

where the *Oldroyd* derivative

$$\frac{D\sigma^p_{ij}}{Dt} \equiv \frac{\partial \sigma^p_{ij}}{\partial t} + v_k \frac{\partial \sigma^p_{ij}}{\partial x_k} - \frac{\partial v_i}{\partial x_k}\sigma^p_{ij} - \frac{\partial v_j}{\partial x_k}\sigma^p_{ij} \tag{6}$$

the De Witt model was used for a mono-component fluid (no solvent) with the the *Jauman* derivative

$$\frac{D\sigma_{ij}}{Dt} \equiv \frac{\partial \sigma_{ij}}{\partial t} + v_k \frac{\partial \sigma_{ij}}{\partial x_k} - \omega_{ik}\sigma_{jk} - \omega_{jk}\sigma_{ik} \tag{7}$$

inserted in Eq. (5) (Re_p=Re, σ^p_{ij}=σ_{ij} in this case).

Here $\sigma, \sigma^p, \sigma^s$ are the mixture, polymer base, and solvent stresses, ω is the vorticity tensor.

As *the initial conditions*, zero values were set to all the dependent variables.

The boundary conditions involved increase of the inlet pressure from 0 up to 1 on the law

$$p_{inlet} = \frac{\alpha t}{1 + \alpha t} \tag{8}$$

to reach a steady flow (cf. Fig. 1), as well as setting the outlet pressure to 0, no-slip conditions at the walls $u_{wall} = v_{wall} = 0$, and the flows symmetry conditions

$$u(0,y) = v(x,0) = \frac{\partial u(x,0)}{\partial y} = \frac{\partial v(0,y)}{\partial x} = 0 \tag{9}$$

evidently following from the flows field symmetry, absence of the momentum flux across the x,y axes, and Eq. (5) applied to the shear stress σ_{xy} equal to 0 at the axes.

The inlet pressure increase intensity parameter α was varied within the limits $1 \div 10$ but such a change did not essentially affect the salient features of the below presented results. All the results shown below involve $\alpha = 1$. In this case we will conditionally agree to consider the time in which the time derivative of the inlet pressure diminishes from its initial value to a fraction of $1.5 \cdot 10^{-3}$ as the *stabilization time*. It is approximately equal to 24.8.

NUMERICAL SOLUTION, DYNAMIC FEATURES

The numerical procedure was essentially based on *the pressure correction method* whose particular implementation was presented in Mackarov[6] together with the formal proof of its convergence. The use of this procedure was approved at AERC2010[5].

First of all, it should be mentioned that *very close solutions* for the Oldroyd-B model *with negligent viscosity of the Newtonian solvent* ($Re_s \geq 10^4 \cdot Re_p$), and the De Witt model were obtained. All the results in the figures below are given for the mono-component UCM model. In this case the polymeric component's Reynolds number is designated *Re*.

This reason of the two models behavior similarity, missing in other problems, is discussed in the Conclusions.

The acceleration phase was found to exhibit specific large-scale flow structures which developed on two distinguished mechanisms:

Large-scale vortex-like structures

Such structures in the form of *a group of vortexes* (usually three) with opposite rotation directions (cf. "diwhirls"[7], i.e., pairs of vortexes rotating in opposite directions) were typically observed in the case of UCM and low (≤ 0.1) Reynolds numbers as in Fig. 2. These

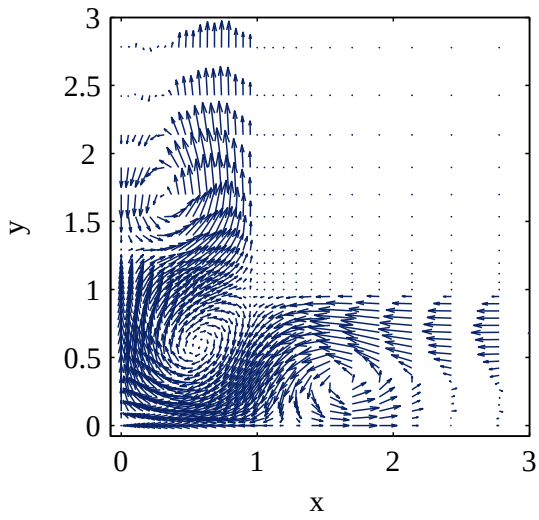

Figure 2. Large-scale vortexes specific for low Reynolds numbers, and a one-component viscoelastic fluid. *Re*=0.05, *Wi*=4, $t \cong 2.7$, the grid has 1200 nodes

essentially non-stationary flow structures were found to periodically rise and damp. Fig. 2 illustrates the top of the intensity, with the flow being like in Fig. 1 between the intensity pics.

It turned out convenient to describe their intensity by a "stability functional", the expression depending on the time derivatives of the flow velocities (N is the total number of the mesh i, j nodes):

$$F(t) = \frac{1}{N} \sum_{i,j} \left(\left| \frac{\partial u_{ij}(t)}{\partial t} \right| + \left| \frac{\partial v_{ij}(t)}{\partial t} \right| \right) \quad (10)$$

Fig 3. shows smooth periodic time dependencies of the observed structures intensity. It is seen from the figure that with moderate *Wi* those oscillations damp up almost completely till the moment of the inlet pressure stabilization (it is encircled at the time axis) whereas with really high *Wi* such kind of the vortexes intensity oscillations can go on much longer, most likely because of essential amounts of the elastic energy accumulated by the fluid.

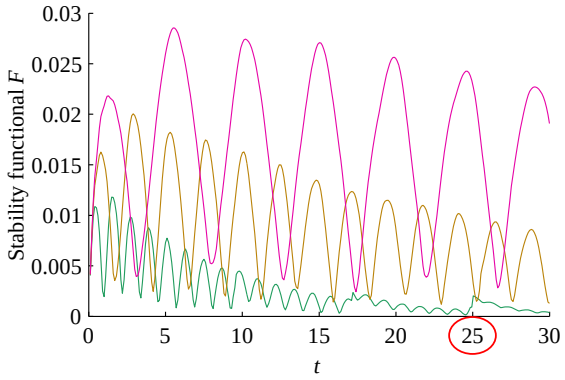

Figure 3. Time dependencies of the stability functional (10) for *Re*=0.05, and *Wi* = 4, 16, and 64 (lower, middle, higher curve). Highlighted is the time moment of the flow conditions stabilization, the grid has 300 nodes.

Less regular flow restructuring

With higher Reynolds numbers (>1) the vortex-like structures disturbing the flows in a non-stochastic manner were no more observed. Instead, as a rule, at some moment the flows were suddenly disturbed in the high-stretch region (near the stagnation point) and got stochastic. This situation is illustrated in Fig. 4. Evidently it is close enough to the classical Reynolds instability.

The time dependency of the functional (10) has also changed: as seen in Fig.5, it is not

oscillatory any more and shows that the flow acceleration phase in the case of this mechanism usually involves a single "burst" of a disturbance which may later damp to form a regular flow or develop then up to the complete loss of stability.

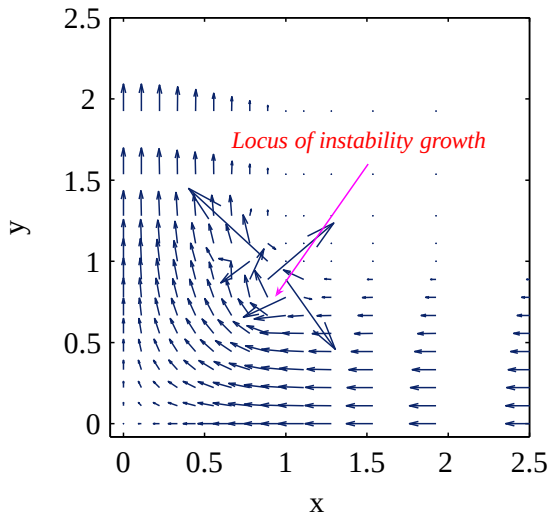

Figure 4. Beginning of sharp instability development specific for moderate and high Reynolds numbers. Re=5, Wi=3, $t\cong$5.3, the grid consists of 300 nodes.

With the presence of the Newtonian solvent with even high Reynolds numbers, or negligent viscosity ($Re_s \geq 10^3 Re_p$) the Oldroyd-B liquid, even with highly viscous viscoelastic base, could be affected by a switch from the first to this second mechanism. So an addition of a Newtonian component can drastically "extinguish" specific elastic oscillatory behavior of the flow at the acceleration phase.

Coming back to the first kind of the found flow structures that were first reported at AERC2010[5], we should point other features of the flow in this situation.

Further analysis of the solution obtained demonstrated that between the picks of the vortexes intensity shown in Fig.3 the flow changed it's general direction.

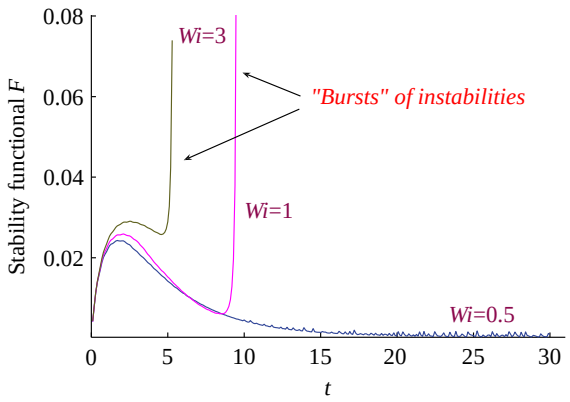

Figure 5.Time dependencies of the stability functional (10) for moderate Reynolds numbers. Highlighted is the stabilization moment, the grid has 300 nodes.

In other words, at times there was a reverse flow like in Fig. 6. This will be analyzed in the next section.

ON THE PHENOMENON OF THE FLOW REVERSE

To analyze the flow reverse phenomenon at the acceleration phase, we will first examine such phases of two simplest flows of the UCM fluid.

Couette flow

As shown in Mackarov[8], the basic system of equations for the UCM fluid flow between two plates (the upper one accelerating on the low similar to (8), and the lower one in rest) is reduced to a single equation for a longitudinal velocity $u = u(t,y)$

$$\frac{\partial^2 u}{\partial t^2} + \frac{1}{Wi}\frac{\partial u}{\partial t} = \frac{1}{WiRe}\frac{\partial^2 u}{\partial y^2} \qquad (11)$$

with conditions

$$u(0,y) = u(t,0) = 0 \qquad (12)$$

$$u(t,1) = \frac{\alpha t}{1+\alpha t} \qquad (13)$$

which in some cases, in particular, with large Wi or small products $Wi \cdot Re$ is close to the

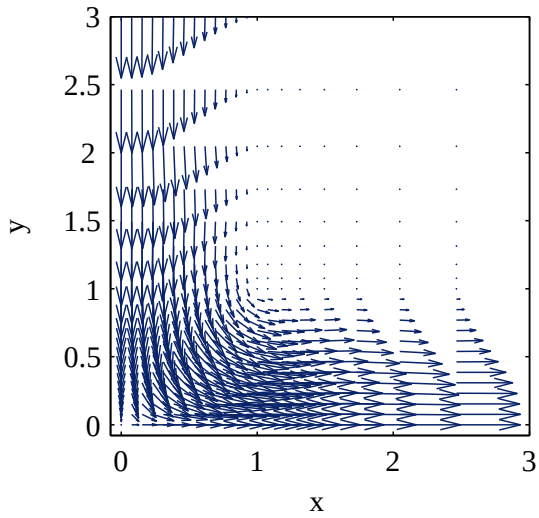

Figure 6. A flow of the UCM fluid whose direction has changed shortly after the phase depicted in Fig. 2. *Re*=0.05, *Wi*=4, $t\cong 3$, the grid has 588 nodes.

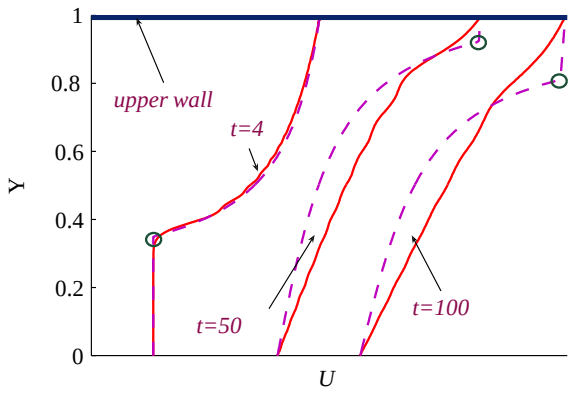

Figure 7. Profiles of the Couette flow in comparison with solution of the wave equation (14). *Re*=1, *Wi*=40. The small circles indicate the points of the wave profiles extremal curvature which move down (the left profile) or up (the right one.

wave equation with the phase wave velocity $c = 1/\sqrt{Wi\,Re}$.

It quite easy to construct the solution of the wave equation with conditions (12)-(13):

$$u_w = V\left(t - \frac{1-y}{c}\right) - V\left(t - \frac{1+y}{c}\right) \quad (14)$$

$$V(p) = \begin{cases} 0 & : \quad p \le 0 \\ V_n(p_n) & : \quad p > 0 \end{cases} \quad (15)$$

here n is the integer part of fraction p/T, $T = 2/c$ - time of the wave double passage over the gap between the plates,

$$p_0 = p - nT \quad (16)$$

$$V_0 = \frac{\alpha\, p_0}{1 + \alpha\, p_0} \quad (17)$$

$$p_k = p_{k-1} + T \quad (18)$$

$$V_k = V_{k-1} + \frac{\alpha\, p_k}{1 + \alpha\, p_k}, \quad k = 1,..n \quad (19)$$

The solutions of the wave equation are given in Fig. 7 (the dashed curves) in comparison with the direct numerical solutions of system (11)-(13). One can see that the wave profile has discontinuities. The *similarity* of two kinds of the solutions is especially evident for the very early instant.

On the ground of a sufficiently large amount of calculations performed, it is possible to come to the conclusion that even for not-too-large *Wi* and not-too-small $Wi \cdot Re$ (of order of 1) the solution of system (11)-(13) is frequently similar to the wave solution (14)-(19). At later stages the flow tends to take the established form with a linear profile (the second and third profiles in Fig. 7) retaining, however, certain features of the wave solution. In particular, the points of discontinuity of the wave solution derivative correspond to the regions of the large curvature of the flow profile that *move up and down* between the plates continually reflecting from them.

Flat Poiseuille flow

The acceleration phase of the flat one-dimensional symmetric flow moving over the x direction within a slot with bounds $y = \pm 1$ due to the rising pressure gradient can be simulated

by the solution of equation

$$\frac{\partial^2 u(t,y)}{\partial t^2} + \frac{1}{Wi}\frac{\partial u(t,y)}{\partial t} = \frac{1}{Wi\,\mathrm{Re}}\frac{\partial^2 u(t,y)}{\partial y^2} - \frac{\partial^2 p(t,x)}{\partial t \partial x} \qquad (20)$$

with conditions

$$u(0,y) = u(t,1) = 0 \qquad (21)$$

$$\frac{\partial u(t,0)}{\partial y} = 0 \qquad (22)$$

(cf. (9))

$$\frac{\partial p(t,x)}{\partial x} = -\frac{\alpha t}{1+\alpha t} \qquad (23)$$

Eq. (20), under the same suppositions about *Re*, *Wi* as with the above considered Couette flow, can be likewise "rendered" to equation:

$$u_p(t,y) = V\left(t - \frac{1-y}{c}\right) - V\left(t - \frac{1+y}{c}\right) - \frac{\alpha t - \ln(1+\alpha t)}{\alpha} \qquad (24)$$

with the solution given by Eqs. (15)-(18), and

$$V_k = V_{k-1} + (-1)^{n-k}\frac{\alpha p_k - \ln(1+\alpha p_k)}{\alpha}, \quad k = 1,\ldots n \qquad (25)$$

As in the previous Couette case, the constructed solution proved quite close to the directly gotten numerical solution of problem (20)-(23) as Fig. 8 shows.

As can be seen from expression (24), this solution has the form of the flow shear distribution moving to and fro across the slot between its wall and the flow axis as a wave.

Condition (22) shows that the reflection from the axis curses the share to change the sign which may change the sign of the shear stress and the flow direction! This possibility is confirmed by the precise numerical solution of this Poiseuille problem and is seen in Fig. 8 where at *t*=6 both numerical and "wave-like" profiles correspond to the reverse of the Poiseuille flow.

Thus, in the case of pure Poiseuille flow we have the flow behavior similar to the case of the cross-slots flow having the regions (not too close to the stagnation point) where Poiseuille-like parabolic profiles arise at certain stages. Evidently, the change of the direction of a cross-slots flow has the reason similar to the one in the Poiseuille case: wave-like propagation of the shear disturbances initiated by the fluid's no-slip at walls and rising pressure gradient due to the elastic nature of the fluid.

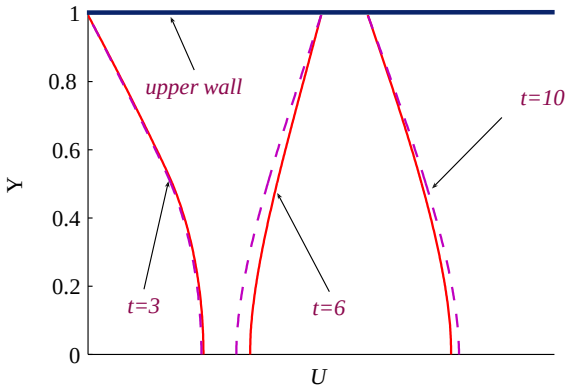

Figure 8. Profiles of the Poiseuille flow (solid lines) in comparison with solution (24) (dashed lines). *Re*=0.1, *Wi*=40.

CONCLUSIONS

So, the study of the acceleration phase of a viscoelastic fluid meeting the Oldroyd-B and De Witt models within cross-slots has elicited a number of the flow features observed previously in experimental and numerical studies as well as some newly found specific dynamic features like a periodic change of the flow direction before the reach of the stationary regime.

It was demonstrated that in the case of a two-component fluid even very low viscosity of the Newtonian solvent can extinct such elastic phenomena as large-scale vortexes, and the

flow reversing.

On the contrary, in the absence of a solvent, when the Oldroyd-B model coincides with UCM, very similar behaviors of this fluid and the De Witt model were observed.

Analysis of stabilization phases of simpler one-dimensional flows and comparison of the results to the case of the cross-slots has shown that the presented oscillatory behavior of the stabilizing flow is underlain by a specific combination of the fluid elastic properties and the role of non-stationary flow conditions.

As to the coincidence between the UCM and the De Witt fluids, which was not the case in some other investigations (Mackarov[9]), probably, the specific of the flow considered here is such that the shear stress is not so large as in the flow considered in this cited work where the De Witt model predicted some specific details of the flow in the regions of high share stresses, such as purely elastic instabilities. This is a matter of future studies.

REFERENCES

1. Arratia, P. et al. (2006) "Elastic Instabilities of Polymer Solutions in Cross-Channel Flow", Phys. Rev. Lett., **96**, id 144502.

2. Poole, R. J. et al. (2007) "Purely Elastic Flow Asymmetries", Phys. Rev. Lett., **99**, 164503.

3. Rocha, G. N. et al. (2009) "On extensibility effects in the cross-slot flow bifurcation", J. Non-Newtonian Fluid Mech., **156**, 58-69.

4. Haward, S. J. (2010) "The rheology of polymer solution elastic strands in extensional flow", Rheol. Acta, **49**, 781-788.

5. Mackarov, I. (2010) "Numerical observation of instabilities in counter flows of viscoelastic fluid", Report on AERC 2010 (Göteborg, Sweden).

6. Mackarov, I. (2009) "Pressure Correction in Simulation of Incompressible Fluid Counter Flows", Internat. J. App. Mech. Eng., **14**, No 3, 791-798.

7. Groisman, A., Steinberg, V. (1997), "Solitary Vortex Pairs in Viscoelastic Couette Flow", Phys. Rev. Lett., **78**, 1460-1463.

8. Mackarov, I. (2001), "Simulation of the phase of establishment of the Couette flow of a viscoelastic fluid", J. Eng. Phys. Thermophys., **74**, 777-781.

9. Mackarov, I. (2003), "Stability of rheometric viscoelastic flow with respect to shear perturbations", Fluid Dyn., **38**, 168-174.